

# Integrated Magnetic Full Wave Converter With Flexible Output Inductor

Liang Yan, Dayu Qu, Brad Lehman  
Department of Electrical and Computer Engineering  
Northeastern University  
Boston, MA 02115

**Abstract**-A new integrated magnetic full wave DC/DC converter<sup>1</sup> is introduced. This converter incorporates an independent output inductor winding within the traditional three-leg magnetic core structure. The inductor winding can be separately designed to control the output current ripple. The cross-sectional area of the inductor core leg can be reduced dramatically. The operation and performance of the proposed circuit were verified on a 100W prototype converter.

## I. INTRODUCTION

Integrated magnetic full wave circuits have been extensively studied [1-3] in an attempt to achieve high power density. These circuits have low switch stress and efficient duty ratio usage. A ‘typical’<sup>2</sup> three-leg magnetic core DC/DC converter is shown in Fig. 1 [3]. As in many integrated magnetic topologies, these full wave circuits exhibit a common character that there is no winding on the inductor leg. Instead, the secondary windings play the role of the equivalent inductor winding in the magnetic energy discharge operating stage, and hence, the secondary windings must satisfy both power transfer and filter functions.

In applications, the elimination of the inductor winding is believed to reduce the copper loss. However, optimum transformer design must keep the balance between copper loss, ferrite loss and total size. For example, in a discrete inductor, increasing both winding turns and gap length can reduce the cross-sectional area, and still maintain the same output current ripple and the flux density. In typical integrated magnetic circuits, the number of secondary winding turns influences the number of primary winding turns, the magnetic core size and the output current characteristics. This places a burden on the secondary winding turn decision. A separate inductor winding can relieve this burden and, therefore, may improve the performance of the transformer. However, the insertion of inductor windings in an integrated magnetic transformer is not arbitrary because the number of inductor winding turns may appear in the voltage transfer function [4] and also influence the continuity of the output current.

This paper presents a new integrated magnetic full wave converter as in Fig. 2. In this full wave circuit, the inductor

winding is retained and can be designed independently from the secondary windings. The added flexibility makes commercial magnetic cores easier to be used, and the transformer design can be optimized. Specifically, the circuit has the following characteristics:

- Retains the original full wave buck mode circuit operation;
- Includes an inductor winding, which does not appear in the input-to-output voltage transfer function;
- The output current is continuous;
- The inductor can be designed specifically to satisfy the current ripple restriction and the magnetic constraints;
- The cross-sectional area of the inductor leg can be much smaller than that of the conventional integrated magnetic circuit to achieve the same output current ripple;
- Achieves 90% power efficiency on an experimental 100W DC/DC converter with an integrated E22 magnetic core.

Section II presents the operation principle of the proposed circuit. Section III introduces the transformer

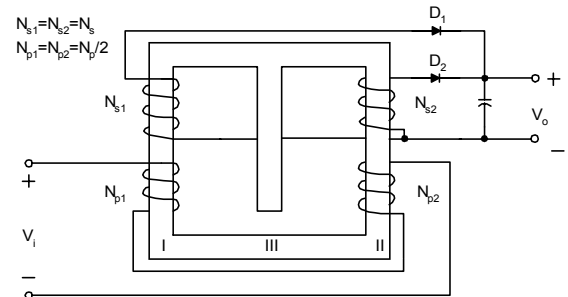


Fig. 1. Conventional Integrated Magnetic Full Wave Circuit

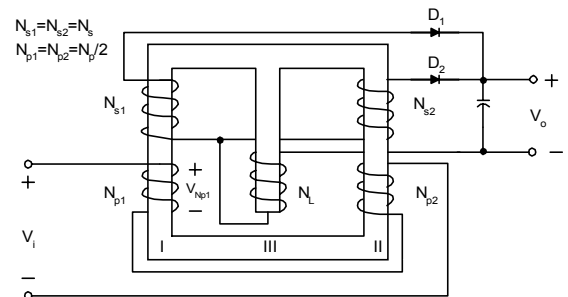


Fig. 2. Proposed Integrated Magnetic Full Wave Circuit (Structure I)

<sup>1</sup> Patent pending.

<sup>2</sup> This paper refers to an integrated magnetic full wave circuit as being ‘typical’ or ‘conventional’ only in the sense that there is no winding on the inductor leg.

design approach. Section IV provides some character comparisons between the conventional and the proposed circuit. An alternative topology of the proposed converter is also introduced. Section V shows the simulation and experimental results for a design example. Section VI gives the conclusion.

## II. OPERATION PRINCIPLE

The basic operation principle of the proposed integrated magnetic full wave circuit in Fig. 2 is similar to the conventional<sup>2</sup> integrated magnetic full wave circuit in Fig. 1. The new converter has two basic operating modes within each half-cycle. The current paths in each mode are illustrated in Fig. 3. In Fig. 4, the magnetic states within each core leg are modeled by using the capacitive modeling method [5-7]. In this model, each current source or sink represents an active winding;  $\dot{\Phi}$  is the flux rate (i.e. the derivative of flux) within each leg;  $P_g$  is the permeance of the gap;  $P_i (i = I \sim III)$  is the permeance of each core leg;  $F$  is the magnetomotive force on the permeance. For a winding on a core leg, two basic relations provide the interface between the magnetic circuit and the electrical circuit:

$$\dot{\Phi} = V/N \quad (1)$$

$$F = NI \quad (2)$$

Gap is abstracted as permeance  $P_g$ :

$$P_g = \mu_0 A/l_g \quad (3)$$

where,

$V$ : the voltage on the winding;

$N$ : the number of winding turn;

$I$ : the current in the winding;

$\mu_0$ : the permeability of the air;

$A$ : the cross-sectional area of the core leg;

$l_g$ : the gap length.

Fig. 5 illustrates the typical operating waveforms. To simplify the analysis, all the devices are assumed to be ideal. The magnetomotive forces on the permeances of the core legs are neglected, i.e. these permeances are assumed to be infinite (compared with the permeance of the gap: see [7] for the accuracy of this assumption). The leakage energy, which is a major implementation problem for most integrated magnetic converters, is not considered at this moment. Let  $V_i$  be as in Fig. 5. The operation principle is explained as follows:

**Mode I:** The input voltage is  $V_i > 0$ . The flux rates  $\dot{\Phi}_{p1}$  and  $\dot{\Phi}_{p2}$ , which are initiated by the primary winding, are shown in Fig. 4. The voltages activated on the secondary

windings force the rectifier  $D_1$  to conduct. The current on the secondary side flows through  $N_L$ ,  $N_{s1}$ ,  $D_1$  and the load. The flux rate difference between *Leg I* and *Leg II* causes flux accumulation in the center leg, which increases the energy storage within the gap. The flux transitions are shown in Fig. 5, where  $\dot{\Phi} = FP$  and  $\dot{\Phi}$  has the same polarity as its corresponding  $F$ .

From Fig. 3 and Fig. 4, the flux rates in each leg can be determined from the magnetic path and the outer circuit as follows:

$$\dot{\Phi}_{p1} = \frac{V_{Np1}}{N_{p1}} \quad (4)$$

$$\dot{\Phi}_{p2} = \frac{V_i - V_{Np1}}{N_{p2}} \quad (5)$$

$$\dot{\Phi}_{L-I} = \dot{\Phi}_{p2} - \dot{\Phi}_{p1} \quad (6)$$

$\dot{\Phi}_{L-I}$  can also be represented from  $N_L$ :

$$\dot{\Phi}_{L-I} = \frac{\dot{\Phi}_{p1}N_s - V_o}{N_L} \quad (7)$$

Since  $N_{p1} = N_{p2} = N_p/2$ , the flux rate in the center leg can then be obtained from (4) to (7):

$$\dot{\Phi}_{L-I} = \frac{(N_s/N_p)V_i - V_o}{N_L + N_s/2} \quad (8)$$

where,

$N_p$ : the total primary winding turn on *Leg I* and *Leg II*;

$N_s$ : the secondary winding turn on *Leg I* and *Leg II*;

$N_L$ : the inductor winding turn on *Leg III*;

$V_i$ : the input voltage;

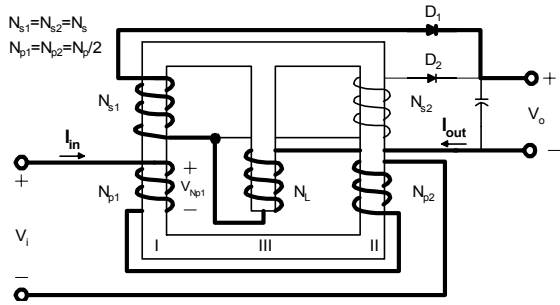
$V_o$ : the desired output voltage.

**Mode II:** The input voltage is  $V_i = 0$ . The primary winding is free. The energy within the gap will release and the entire transformer behaves as an inductor. Both the secondary windings conduct. The two secondary output current paths share the inductor winding. The magnetic state of the transformer is symmetric along the center leg. The flux in the center leg is decreased.

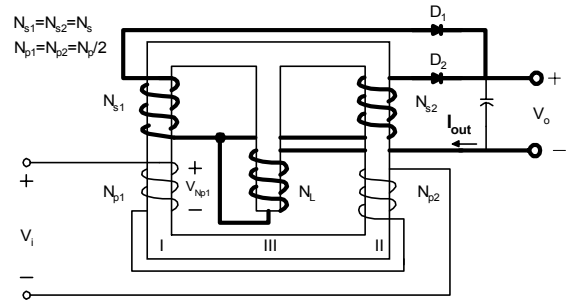
Applying the same method as in Mode I, the flux rate in the center leg is obtained:

$$\dot{\Phi}_{L-II} = \frac{V_o}{N_L + N_s/2} \quad (9)$$

In the next half-cycle, Mode I appears for the winding on the other side. Mode II is exactly the same as in this half-cycle. To derive the input-to-output voltage transfer relation,

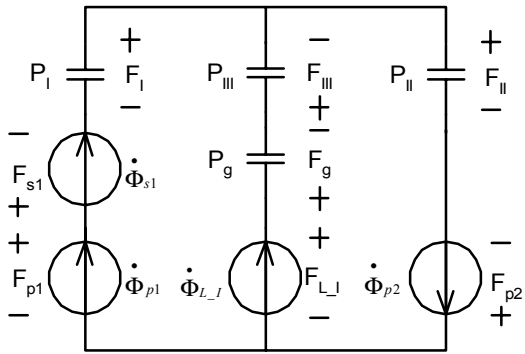


Mode I

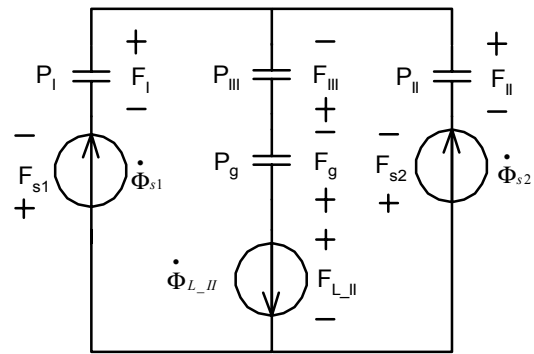


Model II

Fig. 3. Operation Modes



Mode I



Model II

Fig. 4. Analysis Models

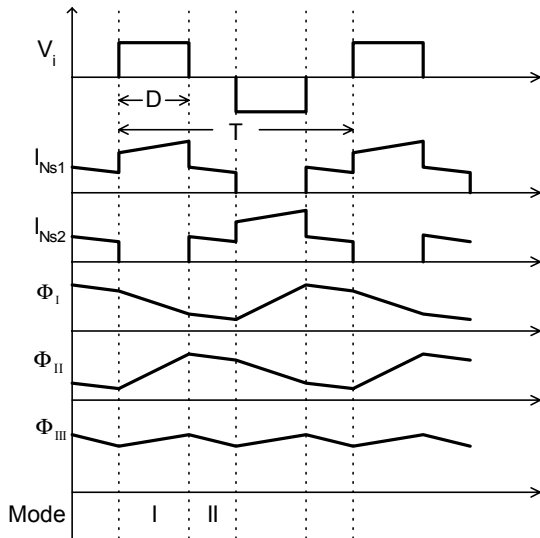


Fig. 5. Operation Waveforms of The New Integrated Magnetic Full Wave Circuit

suppose the duty ratio is equal to  $D$  ( $D < 0.5$ ). Since the flux change should be balanced on the gap in each half cycle:

$$\dot{\Phi}_{L\_I} D = \dot{\Phi}_{L\_II} (0.5 - D) \quad (10)$$

From (8), (9) and (10), the ideal voltage transfer function is

$$\frac{V_o}{V_i} = 2D \frac{N_s}{N_p} \quad (11)$$

This is same as the voltage transfer function of a typical full wave buck mode circuit.

### III. DESIGN APPROACH

Transformer design is vital to achieve favorable performance in any converter, especially for a circuit with integrated magnetics. Design is based on the tradeoff between output current ripple, flux density and magnetic core size. For the design in the newly proposed topology, the following constraints are set in advance:

- Commercial magnetic cores are available for selection;
- The tolerable output current ripple is specified;
- The allowable peak flux density in the core legs is defined.

The purpose of the design is to select the transformer parameters to satisfy the electrical and the magnetic specifications. Specifically, these parameters include

- Magnetic core type and size;
- Total primary winding turn  $N_p$ ;
- Secondary winding turn  $N_s$ ;

- Inductor winding turn  $N_L$ .

In the design, the deterministic parameters are calculated first. Then, the combination of flexible variables is selected. The design may follow three steps:

**Step 1:** Select the primary-to-secondary winding turn ratio  $n = N_p / N_s$ .

The primary-to-secondary winding turn ratio is determined by the input and output voltage specification from (11). Normally,  $n$  is selected to be as large as possible to use the duty ratio more efficiently and to reduce the number of secondary winding turns. However, the line loss and the maximum duty ratio of the controller should be considered to achieve full range input voltage operation.

**Step 2:** Select the magnetic core.

Since the commercial magnetic core is used, it is selected from the available core list according to the output power specification.

**Step 3:** Select the winding turns.

The voltage transfer function is only determined by  $n$ . Once  $n$  is determined, the winding turns are determined by the transformer constraints. The procedure here is to select  $N_s$  and  $N_L$ . This may follow the traditional transformer design method, either by trial and error or by acquiring the optimum combination from the entire parameter lists. The important consideration is to calculate the output current ripple and the peak flux density. The following formulas can be used to verify that these results are within the tolerance.

1. Verify that the output current ripple is within the design specification.

The maximum output current ripple can be derived as

$$I_{L\_d} = \frac{V_o(0.5 - D_{\min})}{f_s P_g (N_L + N_s / 2)^2} \quad (12)$$

where,  $f_s$ : the switching frequency;

$D_{\min}$ : the minimum duty ratio.

2. Verify that the peak flux density in the magnetic core is below the saturation value.

The average flux density in the center leg is

$$B_{c\_av} = \frac{N_L + N_s / 2}{A_c} I_{o\_av} P_g \quad (13)$$

where,  $I_{o\_av}$ : the average output current;

$A_c$ : the cross-sectional area of the center leg.

The average flux density in the outer legs is (identical in the two legs)

$$B_{o\_av} = B_{c\_av} / 2 \quad (14)$$

The maximum flux swing in the center leg is

$$B_{c\_d} = \frac{(N_L + N_s / 2) I_{L\_d} P_g}{A_c} \quad (15)$$

The maximum flux swing in the outer legs is

$$B_{o\_d} = \frac{V_o (N_L / N_s + 1 - D_{\min})}{2 f_s A_o (N_L + N_s / 2)} \quad (16)$$

where,  $A_o$ : the cross-sectional area of the outer legs.

The peak flux density in the center leg is

$$B_{c\_p} = B_{c\_av} + B_{c\_d} / 2 \quad (17)$$

The peak flux density in the outer legs is

$$B_{o\_p} = B_{o\_av} + B_{o\_d} / 2 \quad (18)$$

Both  $B_{c\_p}$  and  $B_{o\_p}$  must be below the saturation value for proper transformer design.

#### IV. TOPOLOGY COMPARISONS

This section compares the previously known integrated magnetic full wave topology in Fig. 1 with the proposed circuit in Fig. 2. An alternative structure of the proposed circuit is also introduced.

##### A. Conventional<sup>2</sup> Topology vs. Proposed Topology

###### 1. Structure Difference

Compared with conventional<sup>2</sup> integrated magnetic full wave topologies, the proposed topology has an additional inductor winding on the center leg. It is obvious that when the inductor winding turn is equal to zero ( $N_L = 0$ ), the proposed circuit is the same as that in Fig. 1. From this point of view, the circuit in Fig. 1 is a special case of the proposed topology.

###### 2. Design Considerations

The transformer design for the new circuit has the flexibility to select the number of inductor winding turns, which can vary from zero to any reasonable number. When the inductor winding turn is small, the secondary winding turn has to be large enough to reduce the output current ripple according to (12). Because the primary-to-secondary turn ratio  $n$  is fixed, the large secondary winding turn leads to large primary winding turn. Both of them cause more copper loss and may also be hard to fit within the magnetic core. On the other hand, it is true that the inductor leg of the magnetic core can be specifically designed to achieve the same performance by large cross-sectional area. However, this increases the cost of designing and manufacturing the specialized magnetic core. At the same time, the additional ferrite volume also increases the ferrite loss, especially in high frequency applications. An example of quantitative

comparisons and choice of inductor winding turns is shown in Section V.

### B. Alternative Structure of Proposed Circuit

#### 1. Structure Comparison

Fig. 6 shows an alternative structure (Structure II) of the proposed circuit. The inductor winding is turned upside down compared with Structure I in Fig. 2. The circuit characteristics can be derived by using the same analysis method.

#### 2. Characteristics Comparison

The operation principle of Structure II is the same as Structure I. The inverse connection of the inductor winding does not change the voltage transfer function. However, the magnetic states within the core are different because the magnetizing direction of the center leg of Structure II is reversed too.

In operation Mode I, primary winding  $N_{p2}$  of Structure I provides both the output power through the secondary winding  $N_{s1}$  and the stored energy in the gap. However, in Structure II it is the opposite primary winding  $N_{p1}$  that provides the energy.

In operation Mode II, these two circuits exhibit different equivalent inductor winding connections as shown in Fig. 7. The equivalent inductor turns are:

$$\text{Structure I} \quad N_L + N_s/2 \quad (19)$$

$$\text{Structure II} \quad N_L - N_s/2 \quad (N_L \geq N_s/2) \quad (20)$$

If comparing the integrated magnetic full wave circuit in Fig. 1 with Structure II, the former is a special case of the latter when  $N_L = N_s$ . This can be verified by replacing  $N_L$  with zero in (19) and replacing  $N_L$  with  $N_s$  in (20). Both lead to the same equivalent inductor turn  $N_s/2$ , which is also the equivalent inductor turn of the conventional circuit.

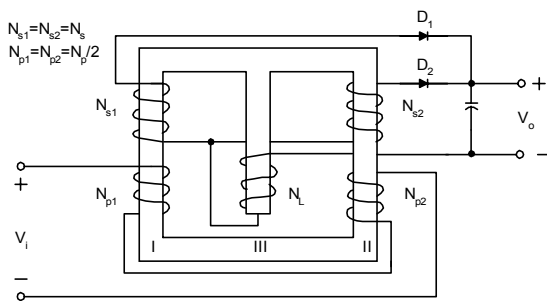


Fig. 6. Alternative Structure of Proposed Integrated Magnetic Full Wave Circuit (Structure II)

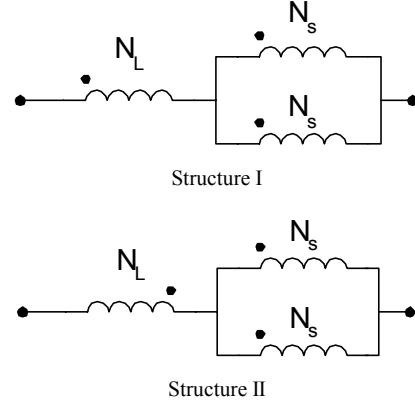


Fig. 7. The Equivalent Inductor Turn

## V. SIMULATION AND EXPERIMENTAL RESULTS

A 100W/3.3V, 150kHz full bridge DC/DC prototype module is designed and built to verify the analysis. The circuit is shown in Fig. 8 and the design specifications are shown in Table I.

### A. Design

The primary-to-secondary winding turn ratio can be calculated as  $n = 9$ . Commercial E22/A160 core is selected. Table II compares the magnetic constraint values, where the inductor winding  $N_L$  varies from zero to three. Table II also shows the different results by varying the secondary winding turn  $N_s$  from two to four. It is obvious that when  $N_L = 0$ , only  $N_s = 4$  leads to the tolerable output current ripple. This is the case of the conventional<sup>2</sup> integrated magnetic circuit. However, the primary winding turn will be  $N_p = 36$ . The reasonable choice of the inductor winding turn is one, i.e.  $N_L = 1$ . Further increase of the inductor winding turn will not reduce the current ripple much and the flux density will be much higher. The secondary winding turn can be two or three. To reduce the loss and size, two-turn is a better choice. If the gap length is decreased to half of its original value, the same current ripple can be achieved. But, the flux density is doubled too. It is not feasible in this design. So, the winding turns are determined:

$$N_{p1} = N_{p2} = N_p/2 = 9, N_s = 2, N_L = 1.$$

The constraint values are:

$$\text{Output current ripple} \quad I_{L\_d} = 10.4A$$

$$\text{Peak flux density in the center leg} \quad B_{c\_p} = 144mT$$

$$\text{Peak flux density in the outer leg} \quad B_{o\_p} = 154mT$$

These are tolerable in a 100W DC/DC module.

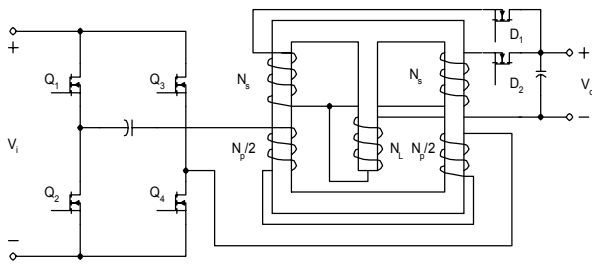


Fig. 8. Experimental Circuit

TABLE I  
CIRCUIT SPECIFICATIONS

Input Voltage	36 V ~ 75 V
Output Voltage	3.3 V
Maximum Output Power	100 W
Switching Frequency	150 kHz

TABLE II  
TRANSFORMER DESIGN CONSTRAINTS  
FROM DIFFERENT WINDING TURNS

OUTPUT CURRENT RIPPLE  $I_{L-d}$  (Amps)

	$N_L = 0$	$N_L = 1$	$N_L = 2$	$N_L = 3$
$N_S = 2$	41.7354	10.4339	4.6373	2.6085
$N_S = 3$	18.5491	6.6777	3.4070	2.0610
$N_S = 4$	10.4339	4.6373	2.6085	1.6694

CENTER LEG PEAK FLUX DENSITY  $B_{c-p}$  (mT)

	$N_L = 0$	$N_L = 1$	$N_L = 2$	$N_L = 3$
$N_S = 2$	103.7	143.6	197.6	255.2
$N_S = 3$	120.1	169.9	226.2	284.6
$N_S = 4$	143.6	197.6	255.2	314.2

OUTER LEGS PEAK FLUX DENSITY  $B_{o-p}$  (mT)

	$N_L = 0$	$N_L = 1$	$N_L = 2$	$N_L = 3$
$N_S = 2$	144.2	153.5	177.0	204.1
$N_S = 3$	121.6	140.9	166.6	194.4
$N_S = 4$	118.0	141.5	168.5	196.9

### B. Simulation

In Fig. 9,  $drive_{14}$  and  $drive_{23}$  are the driving signal of the switches on the primary side.  $I_{primary}$  is the current waveform in the primary winding.  $I_{inductor}$  is the current waveform in the inductor winding.  $V_{ds}$  is the drain-source voltage waveform on the primary switches. This figure shows the operation when the input voltage is 48V and the output current is 30A.

### C. Experiment

To build the circuit, a Philips 3F3 E22/6/16 planar core is selected. Four Si4480 MOSFETs are used as the primary

switches. Three parallel Si4466 synchronous rectifiers are used for each rectification path on the secondary side. The secondary stage uses the controlled synchronous rectification scheme [8, 9]. To keep the flux balance, an isolation capacitor is in series with the primary winding of the transformer.

Fig. 10 is the experimental result of the inductor current. Fig. 11 shows the experimental drain-source voltage waveform of the primary switch and the current waveform in the primary winding. The results verify the analysis. It also shows that the ringing exists due to the leakage inductance. To eliminate the ringing, either phase shift technique or additional active clamp circuit can be used. Fig. 12 shows the result by using an active clamp circuit. The waveform is clean. However, in low power DC/DC converters, the power loss in the additional circuit is often larger than the loss from the ringing. Furthermore, in a full bridge circuit, the voltage on primary switches is naturally clamped by input voltage. The circuit works safely without the clamp circuit and achieves the efficiency as shown in Fig. 13 and Fig. 14 on a copper board with a fan for cooling.

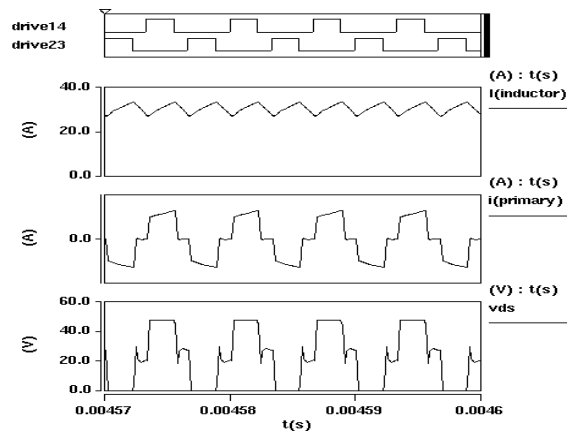
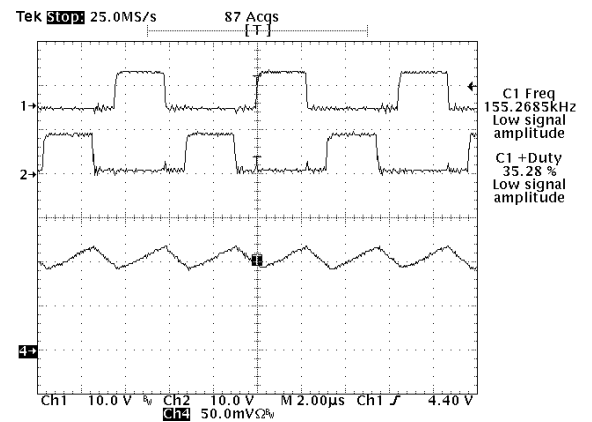


Fig. 9. Simulation Results



Ch 1, Ch 2: Driving Signal;  
Ch 4: Inductor Current.

Fig. 10. Inductor Current

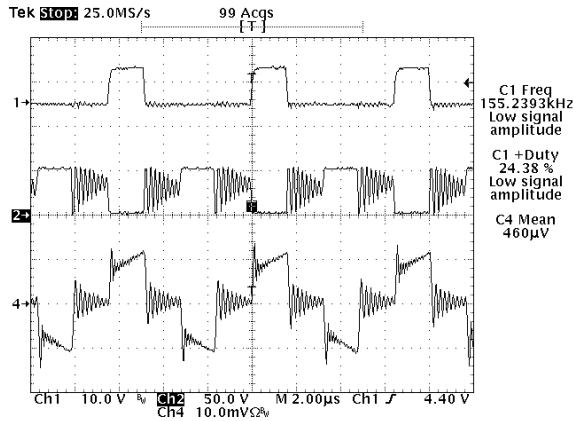


Fig. 11. Primary Current and  $V_{ds}$  of Switch

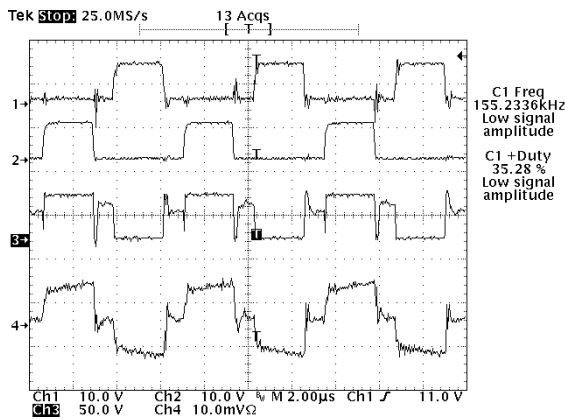


Fig. 12. Primary Current and  $V_{ds}$  of Switch with Active Leakage Energy Recovery Circuit

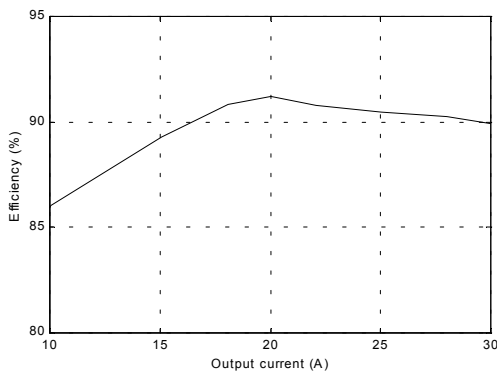


Fig. 13. Total Efficiency vs. Output Current (Input Voltage 48V / Output Voltage 3.3V)

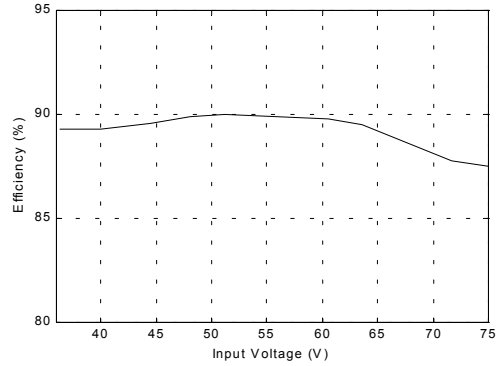


Fig. 14. Total Efficiency vs. Input Voltage (Output Current 30A / Output Voltage 3.3V)

## VI. CONCLUSION

A new integrated magnetic full wave topology is presented. The inductor winding is independent from the circuit voltage transfer function. The transformer can be designed to achieve a compromise between the number of inductor winding turns and the magnetic core size. The operation principle of the circuit is analyzed and the design relations are presented. Simulations and experiments verify the circuit analysis.

## REFERENCES

- [1] G. Q. Morris, "Magnetically Integrated Full Wave DC to DC Converter," *US Patent 5,555,494*, September 10, 1996.
- [2] W. Chen, "Single Magnetic Low Loss High Frequency Converter," *US Patent 5,784,266*, July 21, 1998.
- [3] P. Xu, Q. Wu, P. Wong and F. C. Lee, "A Novel Integrated Current Doubler Rectifier," *IEEE APEC*, 2000, pp. 735-740.
- [4] R. Severns & E. Bloom, *Modern DC/DC Switchmode Power Converter Circuits*, Van Nostrand Reinhold Company, December 1985.
- [5] D. C. Hamill, "Lumped Equivalent Circuits of Magnetic Components: The Gyrator-Capacitor Approach," *IEEE Trans. On Power Electronics*, Vol. 8, No. 2, April 1993, pp. 97-103.
- [6] D. C. Hamill, "Gyrator-Capacitor Modeling: A Better Way of Understanding Magnetic Components," *IEEE APEC*, 1994, pp. 326-332.
- [7] L. Yan, B. Lehman, "Better Understanding and Synthesis of Integrated Magnetics With Simplified Gyrator Model Method," *IEEE PESC*, 2001, pp. 433-438.
- [8] W. Song, B. Lehman, "Driving Method for Synchronous Rectifier of Dual-ended DC/DC Converters," *HFPC*, 2000, pp. 446-451.
- [9] N. Murakami, H. Namiki, K. Sakakibara, T. Yachi, "A simple and efficient synchronous rectifier for forward DC-DC converters," *IEEE APEC*, 1993, pp. 463-468.